Vol. No.5, Issue No. 09, September 2016 www.ijarse.com



MODELING BIDIRECTIONAL CONTACTLESS GRID INTERFACES BASED ON INDUCTIVE POWER TRANSFER WITH A SOFT DC-LINK

Gaddameedi rakesh¹, T. Venu gopal², V. Bhavani³

ABSTRACT

Inductively coupled, bidirectional grid interfaces are gaining popularity as an attractive solution for vehicle-to-grid (V2G) and grid-to-vehicle (G2V) systems. However, such systems conventionally use a large, electrolytic dc-link capacitor as well as a large input inductor, leading to expensive, bulky, and less reliable systems. Although, matrix converter (MC) based bidirectional inductive power transfer (BD-IPT) grid interfaces are proposed as an alternative, implementation of safe and reliable MCs in BD-IPT applications is still a challenge, due to the absence of natural freewheeling methods and higher complexity. As a solution, this paper proposes a new, inductively coupled, bidirectional grid interface, while not a dc-link capacitor and an input inductor, consisting of 2 back-to-back connected converters. In contrast to existing bidirectional grid converters, the proposed system employs a simpler switching strategy with a lower switching frequency. A mathematical model, that predicts the behavior of the introduced system, is additionally given. The feasibility of the proposed technique and also the accuracy of the mathematical model are demonstrated through both simulations results of a 1.1-kW prototype system.

Keywords—DC-link capacitor, electric vehicles (EVs), grid converters, inductive power transfer (IPT), matrix converters (MCs).

I. INTRODUCTION

In recent years, the demand for electric vehicles (EVs) has risen significantly because of many reasons, like improvement in EV technologies, high fuel costs associated with conventional vehicles, and increased awareness on reducing greenhouse gas emissions. Moreover, with the emergence of vehicle-to-grid (V2G) and grid-to-vehicle (G2V) technologies, EVs are proposed as energy storage devices for storage and retrieval of energy for dynamic demand management [1]–[3].

Currently, hard-wired bidirectional grid interfaces are used for grid integration of EVs. Although hard-wired interfaces between EVs and also the utility grid are simple, they must be suitably isolated to avoid the risk of shock hazards [4]. However, they still increase the risk of electrocution, significantly under wet environments and harsh weather conditions, like snow and ice, making safe use of hard-wired interfaces practically difficult. Since these particular grid interfaces are equipped with long cables, they'll also be inconvenient and inflexible [5]. In recent years, inductive power transfer (IPT) has emerged as a favored technique for supplying contactless

Vol. No.5, Issue No. 09, September 2016 www.ijarse.com



power for a wide range of applications [6]–[12]. In contrast to hardwired interfaces, contactless grid interfaces based on bidirectional inductive power transfer (BD-IPT) technology have shown substantial promise as an attractive solution for V2G and G2V applications because of their higher galvanic isolation, flexibility, and efficiencies comparable to hard-wired systems [9]. However, the operating frequencies of BD-IPT systems are usually much higher than the utility grid frequency. Therefore, contactless grid integration of EVs for V2G or G2V applications involves a single or multistage frequency conversion, using one or more bidirectional power electronic converters. Furthermore, as a typical BD-IPT system includes a sixth or eighth order, high-frequency resonant network [13], control of such systems is more demanding in contrast to traditional applications. However, 2 differing kinds of bidirectional device topologies that are used for grid integration of BD-IPT systems are presented in the literature [14], [15].

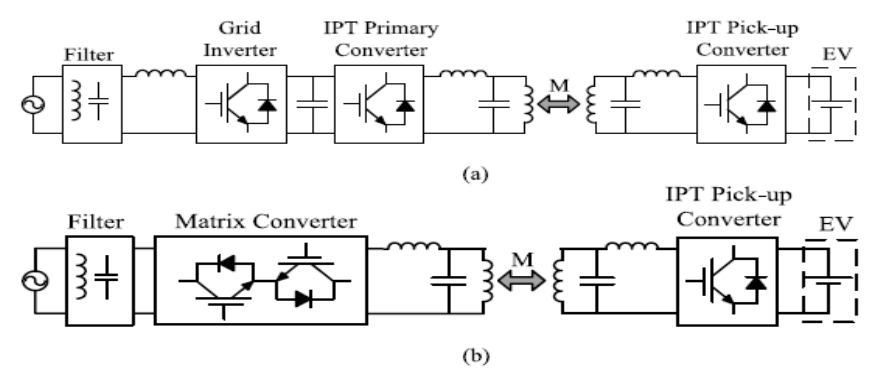


Fig.1. Converter topologies for grid integration of BD-IPT systems (a) grid inverter-based system (b) MC-based system.

Out of the 2 topologies reported, one that is reported in [14] consists of a two-stage energy conversion method, using 2 converters on the primary side of the BD-IPT system, as shown in Fig. 1(a). The converter on the front end, that is referred to because the grid inverter, is driven by high-frequency PWM signals based on proportional-resonant or direct-quadrature controllers. By doing thus, it converts the utility grid ac voltage to a dc voltage and maintains the converted dc voltage at a relatively constant value.

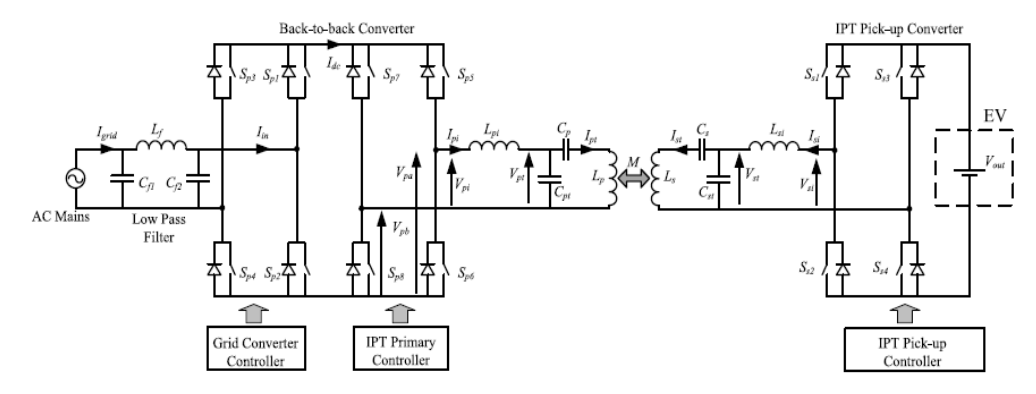


Fig.2. Proposed converter topology for grid integration of BD-IPT systems.

Vol. No.5, Issue No. 09, September 2016 www.ijarse.com



The device on the back end, called the IPT primary converter, and then converts the constant dc voltage at the intermediate dc-link to an ac voltage at the resonant frequency, in order to drive the resonant network. Hence, this system necessitates a large electrolytic dc-link capacitor and an input inductor for minimizing voltage ripple at the intermediate dc-link and reducing input current ripples, respectively. Inclusion of these 2 energy storage elements makes the system bulky and more expensive. in addition, numerous external factors like, kind of dielectric material used, operating and storage temperatures, contribute to determining the life time of the dclink capacitor. As a result, inclusion of the dc-link capacitor compromises the reliability of the entire system. Alternately, matrix converter (MC)-based bidirectional inductively coupled grid interfaces are proposed in [15]. Being a direct ac-ac converter, the MC is able to convert low frequency ac voltage on the grid side to a high-frequency ac voltage at the converter output. Consequently, this eliminates the necessity of a large input inductor, dc-link capacitor, and also the additional ac-dc conversion stage in the grid inverter based system as shown in Fig. 1(b). Hence, the MC-based system becomes less expensive and more compact in comparison to a conventional grid inverter-based system. However, current commutation of the MC should be controlled using precise and complicated multistep commutation algorithms. Thus, the complexity of the controller of the MCbased system becomes significantly higher, particularly in BD-IPT applications wherever high frequency, highorder resonant networks are present. Hence, reliable and safe operation of the MC is very demanding.

This paper presents an inductively coupled, bidirectional grid interface scheme that overcomes aforementioned drawbacks of existing systems. The proposed system performs 2-stage energy conversion using two converters, without having a constant or stiff dc-link voltage. Therefore, it eliminates the requirement of a large dc-link capacitor. Due to the absence of the dc-link capacitor, a voltage with a large ripple, which is close to the peak of the grid voltage, is manifested in the dc-link voltage of the given system. Hence, the dc-link of the proposed system is referred to as soft dc-link during this paper. The large input inductor has also been excluded by exploiting the inherent current source nature [9] of the parallel resonant circuit. This attributes to a more compact, reliable, and a less expensive system in comparison to conventional grid inverter-based systems. Moreover, in contrast to the present systems, the front end converter is operated employing a simple switching strategy at utility grid frequency, with near-zero-voltage switching. The paper presents comprehensive mathematical analyses and compares theoretical results with those obtained from a 1.1-kW MATLAB simulation model to demonstrate system's capability to realize regulated bidirectional power flow to/from the grid. Furthermore, the total harmonic distortion (THD) of the grid current, power factor, and also the efficiency of the overall system are given to investigate the performance of the proposed scheme. Results suggest that the proposed bidirectional inductively coupled grid interface is efficient, reliable, and easy to implement, and suitable for contactless V2G and G2V applications.

II. PROPOSED GRID-INTEGRATED BIDIRECTIONAL IPT SYSTEM

A schematic of the proposed grid integrated BD-IPT system is shown in Fig. 2. the primary side of the system consists of 2 converters that are connected during a back-to-back configuration. The front end converter, which is referred to as the grid converter, is directly interfaced with the utility grid, due to current source nature of the

Vol. No.5, Issue No. 09, September 2016 www.ijarse.com



tuned inductor–capacitor–capacitor– inductor (LCCL) resonant network [13], an input inductor isn't needed for controlling the grid current. Therefore, the large input inductor is eliminated. Regardless of the direction of the power flow, switching devices Sp1 and Sp4 remain ON throughout the complete positive half of the grid voltage, whereas, during the negative half cycle of the grid voltage Sp2 and Sp3 remain ON. However, this needs precise detection of zero-voltage crossings of the utility grid voltage, however measuring voltages accurately near zero is practically a difficult task. To make the situation worse, incorrect detection of zero-voltage crossings can lead to a phase-to-neutral short circuit through the grid converter. When the grid voltage, $V_{\text{grid}} >_{-} V + \text{and } V_{\text{grid}} <_{-} V -$, the grid converter is said to be in normal operation. Due to the switching of $S_{P1} - S_{P4}$ as shown in Fig. 3, a dc voltage with a ripple of V_{in} is formed in the dc-link, where V_{in} is the peak of the utility grid voltage. Thus, the grid converter functions as a rectifier at utility grid frequency when the power flows from the grid to the EV, while it operates as an inverter when the power flow is in reverse direction, i.e., from the EV to the grid.

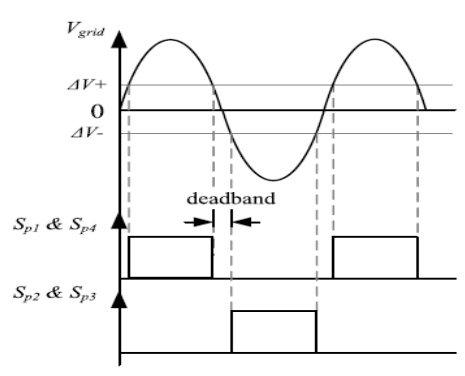


Fig. 3. Operation of $Sp \ 1 - Sp \ 4$ with deadband.

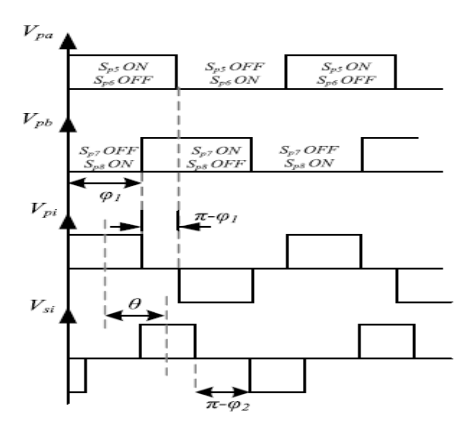


Fig. 4. Voltages produced by IPT primary and pick-up converters.

The IPT primary converter in Fig. 2 is employed for converting the dc voltage across the soft dc-link into an ac voltage at resonant frequency. Switching devices S_{P5} and S_{P6} of the IPT primary converter are switched at the resonant frequency f_T , with a duty cycle of 50%, to generate a square wave voltage V_{Pa} as shown in Fig. 4. In order to generate V_{Pb} , S_{P7} , and S_{P8} are operated at f_T with a 50% duty cycle but with a phase delay ϕ_1 with respect to V_{Pa} , which is referred to as the primary phase modulation. Due to the difference between V_{Pa} and V_{Pb} ,

Vol. No.5, Issue No. 09, September 2016 www.ijarse.com



an ac voltage V_{pi} at fr manifests at the output of the primary IPT converter, and the effective value of V_{pi} depends on the primary phase modulation. Subsequently, V_{pi} produces a current I_{pt} in the primary winding L_p which is loosely coupled to the pick-up winding L_s . The IPT pick-up converter in Fig. 2 is also operated using the same principle, but with a relative phase shift θ with respect to V_{pi} , as illustrated in Fig. 4. This converts the dc voltage V_{out} , which represents an EV for simplicity, to an ac voltage V_{si} at the same resonant frequency fr. As a result, a current I_{st} in the pick-up winding L_s is generated. Contactless power transfer takes place across the air gap between the primary and the pick-up windings due to the mutual coupling between them, and the relative phase angle between I_{pt} and I_{st} , which essentially depends on θ , determines the magnitude and direction of power flow. In order to maintain the power factor of the system near unity, the relative phase angle θ is maintained at • I_{st} 90° [9], and hence, the regulation of power is accomplished by controlling the pick-up phase modulation θ 2.

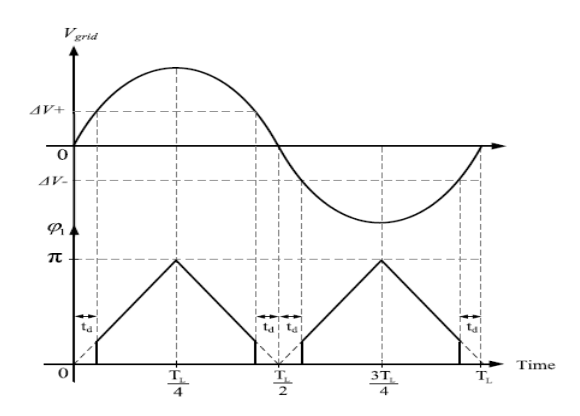


Fig. 5. Regulation of primary phase modulation $\phi 1$ with grid voltage.

Furthermore, as the grid converter disconnects the BD-IPT system from the utility grid during the deadband, it is essential for the primary IPT converter to interrupt the flow of energy from/to the soft dc-link to prevent an undershoot or overshoot of the soft dc-link voltage during this particular time frame. Therefore, the primary phase modulation ϕ_1 is retained at 0° and, consequently, the IPT primary converter short circuits the primary LCCL resonant network to decouple it from the pickup. Hence, no power transfer takes place between the primary and the pick-up systems during the deadband. In order to reduce grid current THD, the technique reported for MC-based grid connected BD-IPT systems, has been adopted in the proposed back-to-back converter (BTBC)-based BD-IPT system. This technique basically modulates I_{pi} by controlling primary phase modulation ϕ_1 , so that grid current I_{grid} gets modulated. For that reason, ϕ_1 is linearly regulated with the phase of V_{grid} as shown in Fig. 5, where t_d represents the duration of the deadband, and $V_{grid} = V_{in} \sin(\omega t_i)$. Moreover, to prevent the injection of high-frequency harmonic currents to the grid, a small low-pass filter as shown in Fig. 2 was employed between the grid converter and the utility grid.

Vol. No.5, Issue No. 09, September 2016 www.ijarse.com



III. MATHEMATICAL MODEL

Due to the operation of the grid converter, a dc voltage of $V_{\rm in}$ /sin ($\omega L t$)/ is produced across the soft dc-link, where ωL represents the frequency of the utility grid voltage. Hence, the IPT primary converter produces an ac voltage at its output, which can be given by

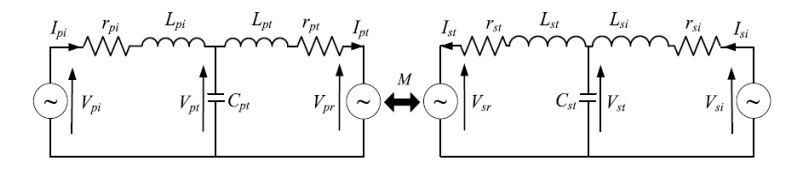


Fig. 6. Reduced LCL network.

$$V_{pi} = V_{\text{in}} \left| \sin \left(\omega_L t \right) \right| \frac{4}{\pi} \sum_{n=1,3}^{\infty} \frac{1}{n} \cos \left(n \omega_T t \right) \sin \left(\frac{n \varphi_1}{2} \right) \tag{1}$$

where $\omega \tau$ is the angular resonant frequency.

Furthermore, an expression for the variation of ϕ_1 can be developed using Fourier series as

$$\varphi_{1}(t) = \left[\frac{\pi}{2} + \frac{4}{\pi} \sum_{n_{1}=1,3,\dots}^{\infty} \frac{(-1)^{\frac{n_{1}-1}{2}}}{n_{1}^{2}} \sin\left\{ 2n_{1}\omega_{L}\left(t - \frac{T_{L}}{8}\right) \right\} \right]$$

$$\times \left[\left(1 - \frac{4t_d}{T_L} \right) + \frac{2}{\pi} \sum_{n_2=1}^{\infty} \frac{\frac{(-1)^{n_2-1}}{n_2} \sin\left(4n_2 \pi \frac{t_d}{T_L}\right)}{\cos\left\{2n_2 \omega_L \left(t - \frac{T_L}{4}\right)\right\}} \right]. \tag{2}$$

The output voltage of the pick-up converter can also be derived as

$$V_{si} = V_{\text{out}} \frac{4}{\pi} \sum_{n=1,3...}^{\infty} \frac{1}{n} \cos(n\omega_T t + n\theta) \sin\left(\frac{n\varphi_2}{2}\right).$$
 (3)

In order to simplify the *LCCL* network shown in Fig. 2, the equivalent impedance Z_{pt} of L_p and C_p at an angular frequency ω can be defined as $Z_{pt} = L_p\omega - 1/\omega C_p$. Z_{pt} is inductive for the frequencies considered in this paper and hence, $L_{pt}\omega = Z_{pt} = L_p\omega - 1/\omega C_p$ where L_{pt} represents the equivalent inductance of L_p and C_p . Therefore, L_{pt} can be written as

$$L_{pt} = L_p - \frac{1}{\omega^2 C_p}. (4)$$

Similarly on the pick-up side, L_s and C_s can be reduced by defining another equivalent inductor L_{st} , which is given by

$$L_{st} = L_s - \frac{1}{\omega^2 C_s}. ag{5}$$

Therefore, the LCCL network can be reduced to an inductor—capacitor—inductor (LCL) network, as depicted in Fig. 6. The mutual coupling M between L_p and L_s can be expressed as $M = k_L_pL_s$, where k is the coefficient of coupling. Therefore, the induced voltages V_{pr} and V_{sr} of the primary and the pick-up networks can be derived as follows:

$$V_{pr} = j\omega M I_{st} \tag{6}$$

Vol. No.5, Issue No. 09, September 2016 www.ijarse.com

a unity magnitude.



$$V_{sr} = j\omega M I_{pt}. (7)$$

The currents I_{pi} , I_{si} , I_{pt} , and I_{st} for an LCL network are derived in [13] as given below

$$I_{pt} = \frac{1}{K} \begin{bmatrix} I_{\text{in}} \frac{Z_{p}}{Z_{p} + j\omega L_{pt} + r_{pt}} \\ +I_{\text{out}} \frac{j\omega MZ_{s}}{(Z_{p} + j\omega L_{pt} + r_{pt})} & (Z_{s} + j\omega L_{st} + r_{st}) \end{bmatrix}$$

$$(8)$$

$$I_{st} = \frac{1}{K} \begin{bmatrix} I_{\text{out}} \frac{Z_{s}}{Z_{s} + j\omega L_{st} + r_{st}} \\ +I_{\text{in}} \frac{j\omega MZ_{p}}{(Z_{p} + j\omega L_{pt} + r_{pt})} & (Z_{s} + j\omega L_{st} + r_{st}) \end{bmatrix}$$

$$I_{pi} = \frac{1}{Z_{pr} + j\omega L_{pi} + r_{pi}} [-I_{pr}Z_{pr} + V_{pi}]$$

$$I_{si} = \frac{1}{Z_{sr} + j\omega L_{si} + r_{si}} [-I_{sr}Z_{sr} + V_{si}]$$

$$(10)$$

Thus, I_{dc} can be written as a product of I_{pi} and a function $f_{primary}(t)$ that represents the operation of the IPT primary converter. According to Fig. 4, $f_{primary}(t)$ is a function that follows the exact shape of V_{pi} , however, with

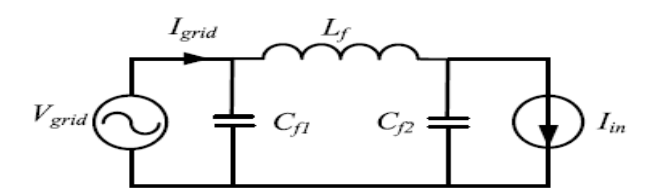


Fig. 7. Current source model of the proposed system with the input filter.

Nevertheless, due to the low-pass filter, higher order frequency components of I_{in+} will be filtered out from the grid current I_{grid} . Therefore, only the fundamental frequency component of I_{in+} will be considered henceforth. As I_{in} is a current source, the entire system can be reduced to Fig. 7. From Fig. 7and by analyzing the dc component and the

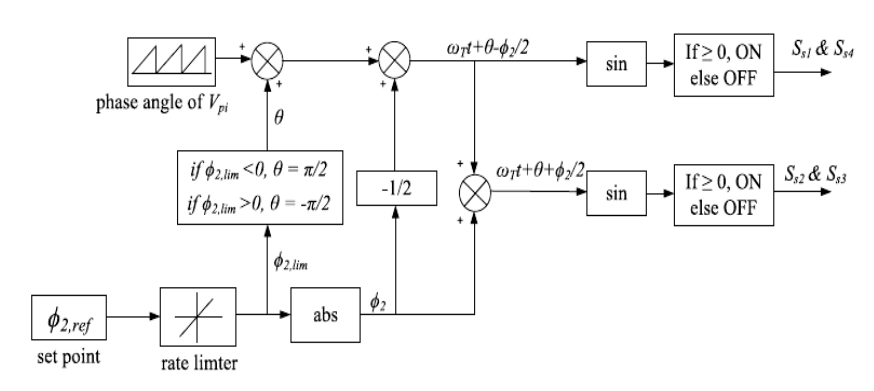


Fig. 8. Block diagram of the IPT pick-up controller.

Vol. No.5, Issue No. 09, September 2016 www.ijarse.com



IV. CONTROL SYSTEM

An open loop control system is introduced to the pick-up side to control the magnitude and direction of the power flow of the proposed system. The block diagram of the pick-up controller is presented in Fig. 8. Based on the amount of power required, the corresponding pick-up phase modulation ϕ_2 can be calculated using for $\theta = \frac{1}{\pi}/2$, and set as the reference pick-up phase modulation $\phi_{2,\text{ref}}$ for the pick-up controller. For power flow from the primary to the pick-up, $\phi_{2,\text{ref}}$ should be positive, while for power flow from the pick-up to the primary, $\phi_{2,\text{ref}}$ should be set as a negative value. Therefore, $\phi_{2,\text{ref}}$ varies between 0 and π radians for power flow from the primary to the pickup with $\theta = -\pi/2$, whereas it is confined between 0 and $-\pi$ radians when the power flow is from the pick-up to the primary. To ensure a smooth transfer of the set point from one value to another, $\phi_{2,\text{ref}}$ is passed through a rate limiter with a predefined value. The absolute value of the rate limited $\phi_{2,\text{ref}}$ occurs to be the pick-up phase modulation for the IPT pick-up converter, as seen from Fig. 8. Furthermore, the phase angle of the primary converter output voltage V_{pi} is employed as an input to the pickup controller to accurately maintain the required phase shift θ of the pick-up output voltage. The resulting pick-up phase modulation ϕ_2 is then divided into $-\phi_2/2$ and $\phi_2/2$ on the time axis, and each pair of switches are operated as expounded in Fig. 8.

TABLE I
PARAMETERS OF THE PROTOTYPE BD-IPT SYSTEM

Parameter	Value
V _{in} (Peak Grid Voltage)	325 V
$V_{ m out}$	200 V
L_{pi} and L_{si}	$99 \mu H$
L_p and L_s	$155 \mu H$
\dot{C}_{pt} and C_{st}	$0.66 \mu F$
C_p and C_s	$1.16 \mu F$
r_{pi} and r_{si}	$12 \text{ m}\Omega$
r_{pt} and r_{st}	$30 \text{ m}\Omega$
\vec{L}_f	$80 \mu H$
C_{f1}	$3.3 \mu F$
C_{f2}	$4.92 \mu F$
k	0.32
Air gap	150 mm
f_T	20 kHz
Grid frequency	50 Hz

V. SIMULATION RESULTS

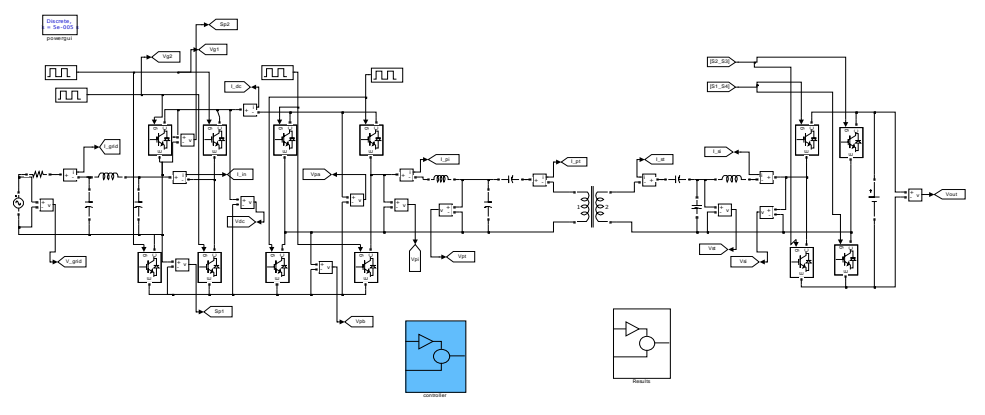


Fig.9. Simulation model for grid integration of BD-IPT systems.

Vol. No.5, Issue No. 09, September 2016 www.ijarse.com



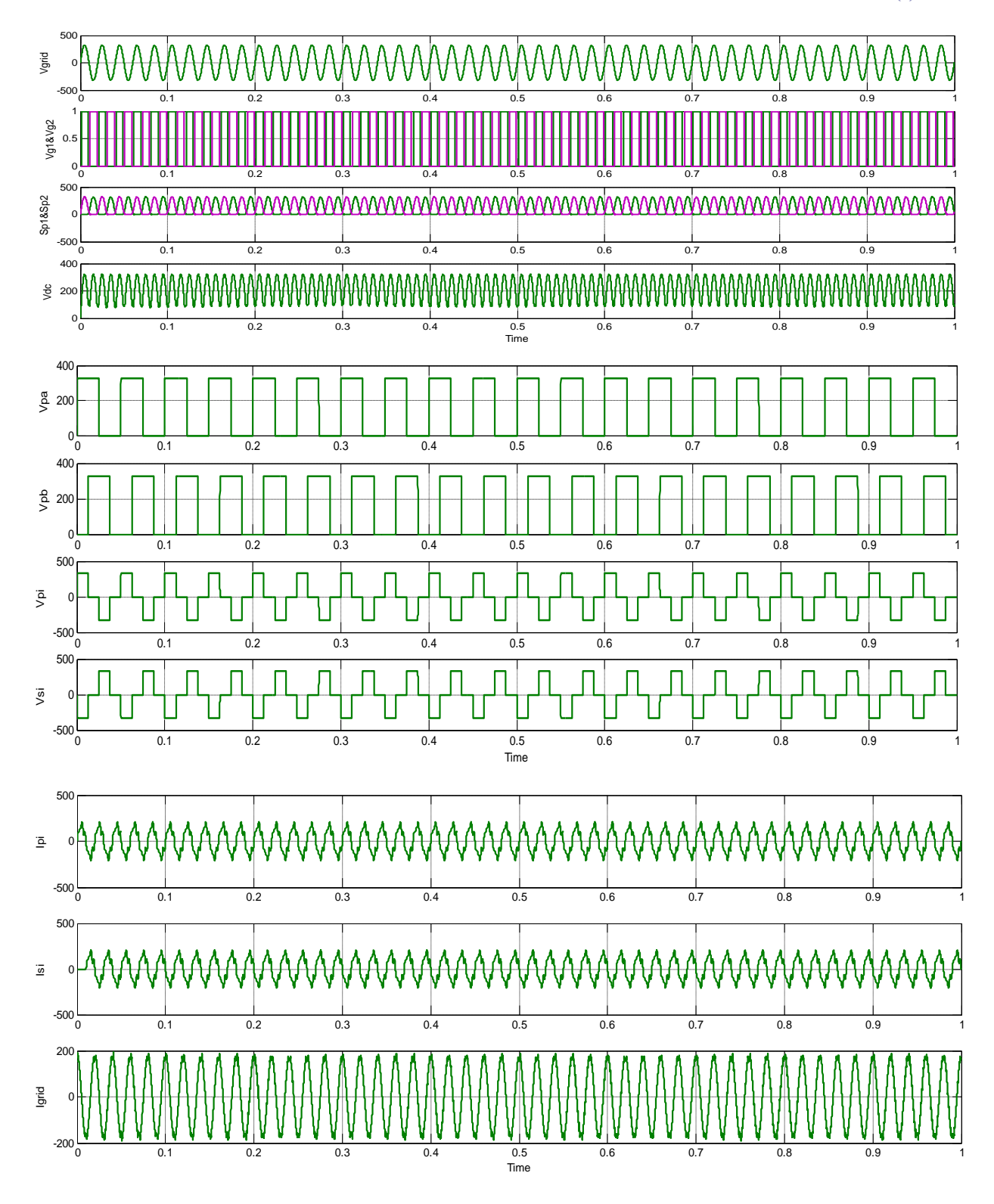


Fig. 10. Simulation results for IPT primary and pick-up converters at $\phi 2 = \pi$ and $\theta = -\pi/2$

Vol. No.5, Issue No. 09, September 2016 www.ijarse.com



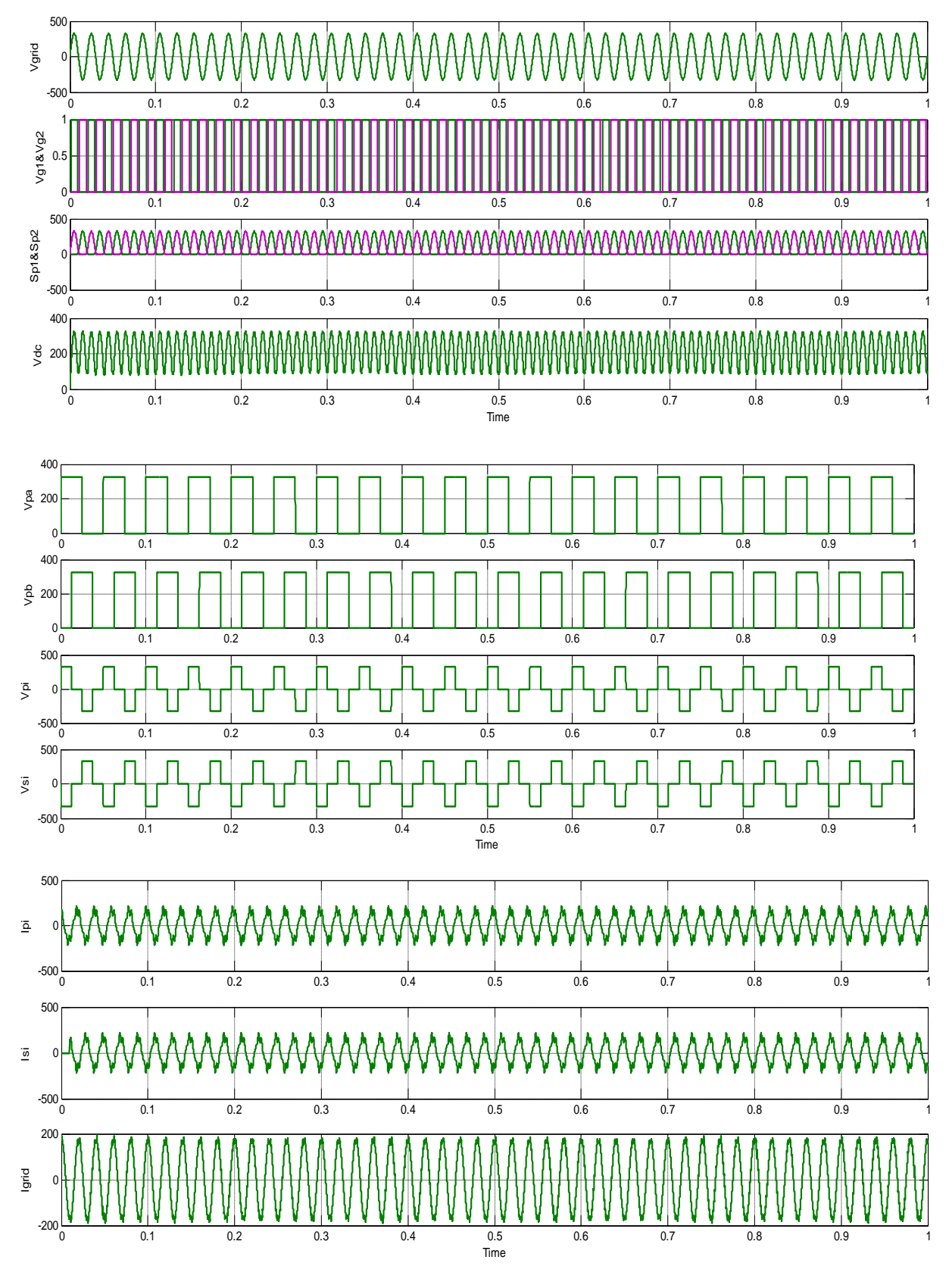


Fig.11 Simulation results for grid side at $\phi 2 = \pi$ and $\theta = -\pi/2$

Vol. No.5, Issue No. 09, September 2016 www.ijarse.com



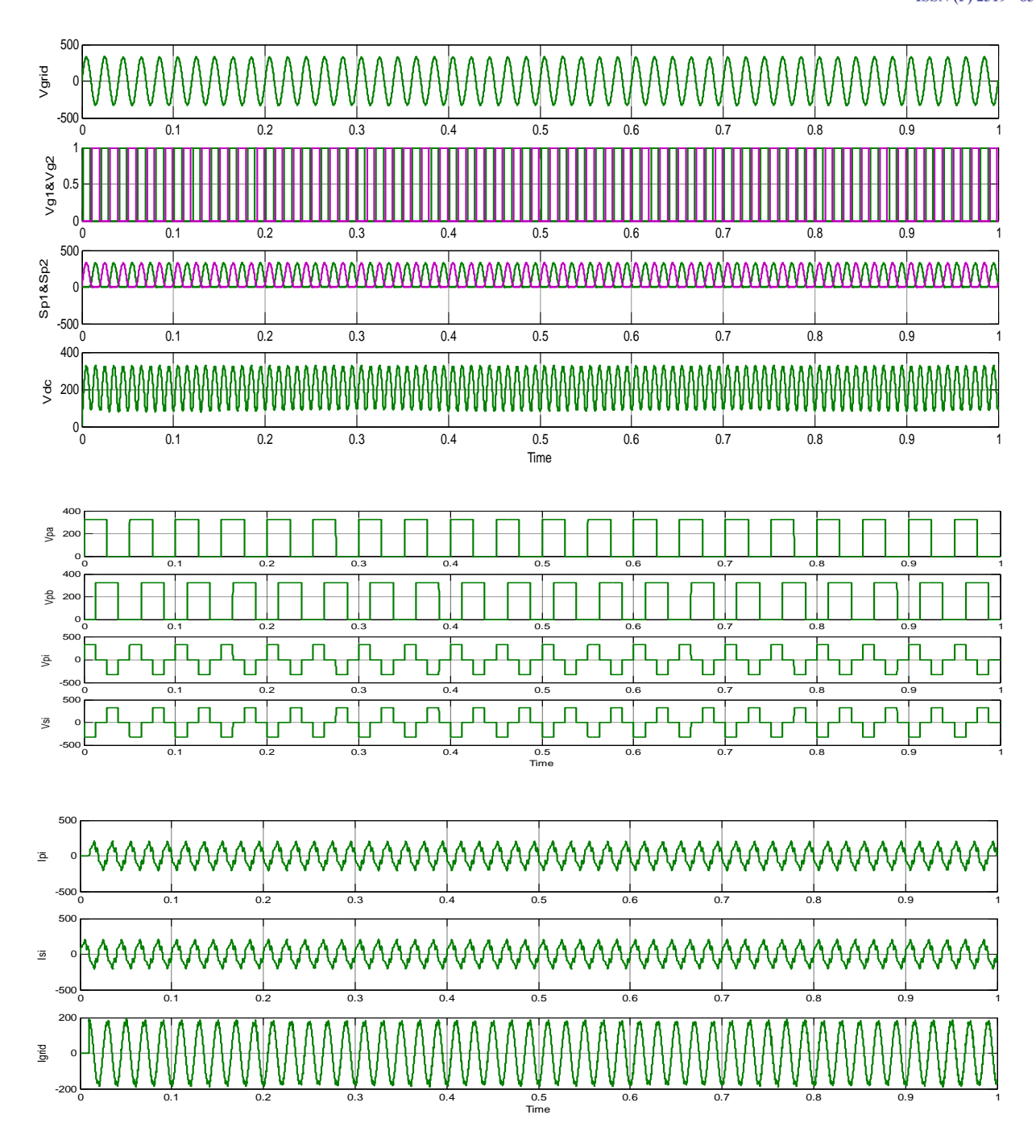


Fig.12 Simulation results for IPT primary and pick-up converters at $\phi 2 = \pi/3$ and $\theta = -\pi/2$

VI. CONCLUSION

A dc-link capacitor and an input inductor-free, bidirectional, contactless grid interface, that is based on inductive power transfer (IPT), has been proposed for V2G and G2V systems. The proposed grid interface comprises 2 converters in back to- back configuration, and has the ability to regulate both the magnitude and also the direction of power flow. In contrast to existing systems, the grid converter will be operated at a much lower

Vol. No.5, Issue No. 09, September 2016 www.ijarse.com



switching frequency employing a simpler switching strategy. A mathematical model that may estimate grid currents, converter voltages, and currents has been given. In order to investigate the feasibility of the proposed scheme, as well as the accuracy of the mathematical model, a MATLAB simulation model. Good agreement between theoretical, simulation results validates the accuracy of the proposed mathematical model. Moreover, the THD of the grid current, the power factor, and also the efficiency of the simulation prototype have been investigated for both directions of power flow, and also the results suggest that the system exhibits a steady efficiency profile with reasonably low THD and a unity power factor, throughout the considered operational range.

REFERENCES

- [1] J. Sexauer, K. McBee, and K. Bloch, "Applications of probability model to analyze the effects of electric vehicle chargers on distribution transformers," *IEEE Trans. Power Syst.*, vol. 28, no. 2, pp. 847–854, Oct. 2013.
- [2] M. Etezadi-Amoli, K. Choma, and J. Stefani, "Rapid-charge electric electric estations," *IEEE Trans. Power Del.*, vol. 25, no. 3, pp. 1883–1887, Jul. 2010.
- [3] Z. Wang and S. Wang, "Grid power peak shaving and valley filling using vehicle-to-grid systems," *IEEE Trans. Power Del.*, vol. 28, no. 3, pp. 1822–1829, Jul. 2013.
- [4] M. Yilmaz and P. Krein, "Review of the impact of vehicle-to-grid technologies on distribution systems and utility interfaces," *IEEE Trans. Power Electron.*, vol. 28, no. 12, pp. 5673–5689, Dec. 2013.
- [5] H. Wu, A. Gilchrist, K. Sealy, and D. Bronson, "A high efficiency 5 kW inductive charger for EVs using dual side control," *IEEE Trans. Ind. Informat.*, vol. 8, no. 3, pp. 585–595, Aug. 2012.
- [6] A. W. Green and J. T. Boys, "10 kHz inductively coupled power transferconcept and control," in *Proc. Fifth Int. Conf. Power Electron. Variable- Speed Drives*, Oct. 1994, pp. 694–699.
- [7] S. R. Hui and W. Ho, "A new generation of universal contactless battery charging platform for portable consumer electronic equipment," *IEEE Trans. Power Electron.*, vol. 20, no. 3, pp. 620–627, Jun. 2005.
- [8] P. Si, A. P. Hu, S.Malpas, and D. Budgett, "A frequency controlmethod for regulating wireless power to implantable devices," *IEEE Trans. Biomed. Circuits Syst.*, vol. 2, no. 1, pp. 22–29, Mar. 2008.
- [9] U. K. Madawala and D. J. Thrimawithana, "A bidirectional inductive power interface for electric vehicles in V2G systems," *IEEE Trans. Ind. Electron.*, vol. 58, no. 10, pp. 4789–4796, Oct. 2011.
- [10] J. Huh, S. Lee, C. Park, G.-H. Cho, and C.-T. Rim, "High performance inductive power transfer system with narrow rail width for on-line electric vehicles," in *Proc. IEEE Energy Convers. Congr. Expo.*, Sep. 2010, pp. 647–651.
- [11] J. M. Miller, O. Onar, C. White, S. Campbell, C. Coomer, L. Seiber, R. Sepe, and A. Steyerl, "Demonstrating dynamic wireless charging of an electric vehicle: The benefit of electrochemical capacitor smoothing," *IEEE Power Electron. Mag.*, vol. 1, no. 1, pp. 12–24, Mar. 2014.

Vol. No.5, Issue No. 09, September 2016

www.ijarse.com



- [12] T. Imura and Y. Hori, "Maximizing air gap and efficiency of magnetic resonant coupling for wireless power transfer using equivalent circuit and Neumann formula," *IEEE Trans. Ind. Electron.*, vol. 58, no. 10, pp. 4746–4752, Oct. 2011.
- [13] D. J. Thrimawithana and U. K. Madawala, "A generalized steady-state model for bidirectional IPT systems," *IEEE Trans. Power Electron.*, vol. 28, no. 10, pp. 4681–4689, Oct. 2013.
- [14] R. Miskiewicz, A. Moradewicz, and M. Kazmierkowski, "Contactless battery charger with bi-directional energy transfer for plug-in vehicles with vehicle-to-grid capability," in *Proc. IEEE Int. Symp. Ind. Electron.*, 2011, pp. 1969–1973.
- [15] D. J. Thrimawithana and U. K. Madawala, "A novel matrix converter based bi-directional IPT power interface for V2G applications," in *Proc. Energy Conf. Exhib.*, Dec. 2010, pp. 495–500.